African Journal of Marine Science

ISSN: 1814-232X (Print) 1814-2338 (Online) Journal homepage: http://www.tandfonline.com/loi/tams20

Annual cycle of the upper-ocean circulation and properties in the tropical western Indian Ocean

M Manyilizu, P Penven & CJC Reason

To cite this article: M Manyilizu, P Penven & CJC Reason (2016) Annual cycle of the upper-ocean circulation and properties in the tropical western Indian Ocean, African Journal of Marine Science, 38:1, 81-99

To link to this article: http://dx.doi.org/10.2989/1814232X.2016.1158123

Published online: 27 Apr 2016.

African Journal of Marine Science 2016, 38(1): 81–99
Printed in South Africa — All rights reserved

AFRICAN JOURNAL OF MARINE SCIENCE
ISSN 1814-232X EISSN 1814-2338
http://dx.doi.org/10.2989/1814232X.2016.1158123

Annual cycle of the upper-ocean circulation and properties in the tropical western Indian Ocean

M Manyilizu[1,2]*, P Penven[3] and CJC Reason[1]

[1] *Department of Oceanography, University of Cape Town, Cape Town, South Africa*
[2] *College of Informatics and Virtual Education, University of Dodoma, Dodoma, Tanzania*
[3] *Ifremer, Univ. Brest, CNRS, IRD, Laboratoire d'Océanographie Physique et Spatiale (LOPS), IUEM, Brest, France*
* *Corresponding author, e-mail: majuto.manyilizu@gmail.com*

A regional ocean model was used to simulate the annual cycle of the upper-ocean dynamics and its influence on ocean properties in the tropical western Indian Ocean. Surface winds and heat fluxes from the National Centers for Environmental Prediction (NCEP) reanalysis forced the model (Model_NCEP) with initial and lateral boundary conditions derived from the Simple Ocean Data Assimilation (SODA). The model findings were in good agreement with previous research, satellite and observational data as well as another model configuration forced by Comprehensive Ocean and Atmosphere Data Sets (COADS). The initial and lateral boundary conditions for Model_COADS were extracted from World Ocean Atlas 2001. Anticyclonic wind stress curl occurred to the north of Madagascar, and extended towards the Tanzanian coast throughout the year, leading to Ekman convergence and downwelling in that region. The lowest sea-surface height values during the year occurred between 5° and 12° S with an elongated and contracted shape. The East African Coastal Current (EACC) was in phase with the westward North-East Madagascar Current (NEMC) throughout the year with volume transports peaking in June through July in the model forced by NCEP reanalysis. The variability of the volume transport, ocean currents, temperature and salinity to the north of Madagascar on the path of the NEMC mirrored those in the middle Tanzanian shelf on the path of the EACC throughout the year. The NEMC seemed to influence the water masses on the Tanzanian shelf, with cooler and lower-salinity water in the South-West Monsoon, and warmer and saltier water during the North-East Monsoon.

Keywords: annual cycle, East African Coastal Current, North-East Madagascar Current, North-East Monsoon, ocean dynamics, South-West Monsoon, Tanzanian shelf

Introduction

The tropical western Indian Ocean plays a vital role in socio-economic development of eastern African countries. In coastal Tanzania, fishing is the main food source and contributes 2–5% of national GDP (more in Zanzibar) (Jiddawi and Öhman 2002). Recent discoveries of offshore oil and gas on the southern Tanzanian shelf are expected to boost the country's economy. Shipping through the ports of Dar es Salaam, Zanzibar, Tanga and Mtwara (Figure 1) contributes significantly to the country's GDP, as well as to trade elsewhere in eastern Africa. Such socio-economic activities are influenced by variability in the upper part of the western Indian Ocean. Thus, a better understanding of the annual cycle in the upper ocean, its sea surface height, circulation and volume transport is important not only for scientific progress but also for managing marine fisheries, ecosystems, shipping, and oil and gas extraction.

The upper-ocean circulation in the tropical western Indian Ocean responds to the monsoon winds, with the South Equatorial Current (SEC), the East African Coastal Current (EACC), the Somali Current (SC) and the South Equatorial Counter Current (SECC) dominating the flow. The surface monsoon winds blow generally from the tropical western Indian Ocean (South-West Monsoon) in austral winter (June–September) towards the Indian subcontinent and from the subcontinent towards the tropical south-western Indian Ocean (North-East Monsoon) in austral summer (December–March). Two transition intermonsoonal periods occur in April/May (austral autumn) and in October/November (austral spring). The surface ocean circulation is strongly seasonally reversed in the tropical Indian Ocean (north of 12° S) by these seasonal reversals in surface winds (Schott et al. 2009). In the southern tropical Indian Ocean, Bell (1972) and McClanahan (1988) pointed out that Tanzanian coastal waters and southern Kenyan waters experience downwelling throughout the year; thus, the region is dominated by coral reefs and benthic productivity associated with low-nutrient water. Moreover, within the southern tropical Indian Ocean, the south-east trade winds drive the SEC. The path of this current is more irregular due to the underlying topography and Rossby waves (Maltrud et al. 1998; Gordon and McClean 1999). The SEC is located between 10° and 20° S (Cutler and Swallow 1984; Shenoi et al. 1999) with velocities that rarely exceed 0.3 m s^{-1} (Tomczak and Godfrey 1994). It branches at the central eastern coast of Madagascar (about 18° S) into the North-East Madagascar Current (NEMC) and the South-East Madagascar Current (SEMC), flowing north-westward and southward, respectively. The SEMC transports about 20 Sv to the southern tip of Madagascar,

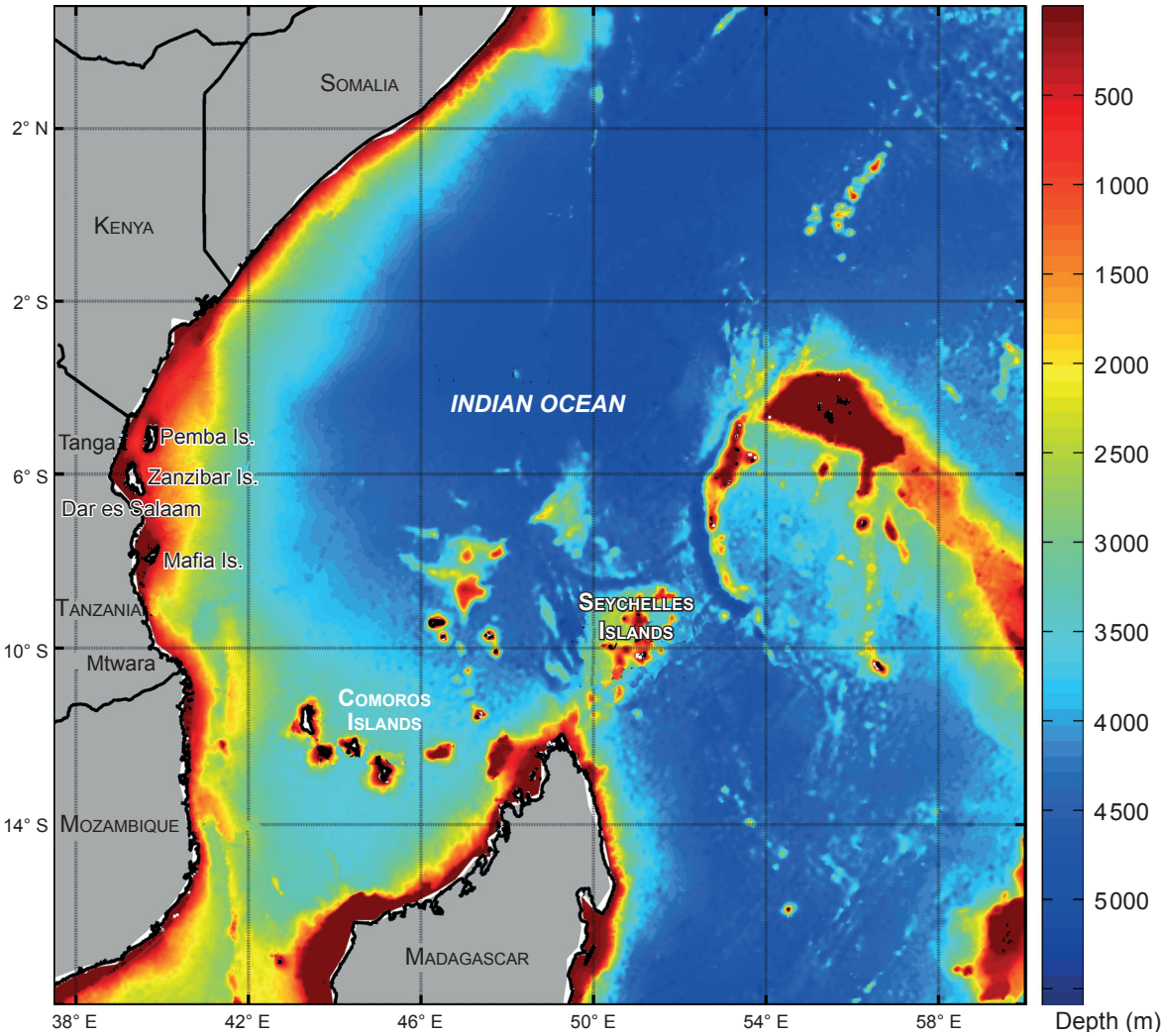

Figure 1: The study domain in the tropical western Indian Ocean and its bathymetry, derived from ETOPO2V2C (www.ngdc.noaa.gov)

where it breaks up into a sequence of eddies and dipoles that migrate to the southern African coast (de Ruijter et al. 2004; Backeberg and Reason 2010). The NEMC transports about 29.60 Sv (SD 8) annually (Swallow et al. 1988; Schott et al. 2009) in the upper 1 000 m with a near-surface speed of 0.7 m s^{-1} (Schott and McCreary 2001). Near the East African coast (at about 10° S), the NEMC splits into the southward eddy-dominated flow through the Mozambique Channel and the northward-flowing East African Coastal Current (EACC) (Pickard and Emery 1990; Tomczak and Godfrey 1994). The annual mean volume transported through the Mozambique Channel (largely migrating anticyclonic eddies), has been estimated as 17 Sv (de Ruijter et al. 2002; Donohue and Toole 2003). This volume is similar to earlier inverse model results of 15 Sv (SD 5) (Ganachaud et al. 2000). The SEC, NEMC and EACC in the southern tropical Indian Ocean are permanent flows, but are strengthened during the South-West Monsoon and weakened in the North-East Monsoon.

During the South-West Monsoon, the trade winds along the East African coast strengthen the EACC up to 2 m s^{-1} from April through October (Newell 1957; Dubi 2000; Julius 2005). Similar speeds of about 2 m s^{-1} with a transported volume of 15 Sv in the upper 100 m were reported in the Indian Ocean Experiment (INDEX, 1976–1979) during April and May of 1979 (Leetmaa et al. 1982; Schott and McCreary 2001). A schematic diagram of the near-surface ocean circulations in the tropical western Indian Ocean during this season is given in Figure 2a. The EACC supplies the northward-flowing SC that flows across the equator, showing different cells and gyres, depending on the time of the season and the driving wind field (Schott et al. 2009). After crossing the equator, part of the SC turns offshore near 4° N with a width in the order of 50–100 km, generating an upwelling process of cooler, nutrient-rich waters (Pickard and Emery 1990; Schott and McCreary 2001; Schott et al. 2009) farther north off the East African coast (Düing and Schott 1978; Smith and Codispoti 1980; Leetmaa et al. 1982). The remaining part of the SC recirculates across the equator, forming the Southern Gyre (Schott et al. 2009) that varies in strength from year to year (Schott et al. 1990). Farther north at 4°–10° N, the Great Whirl

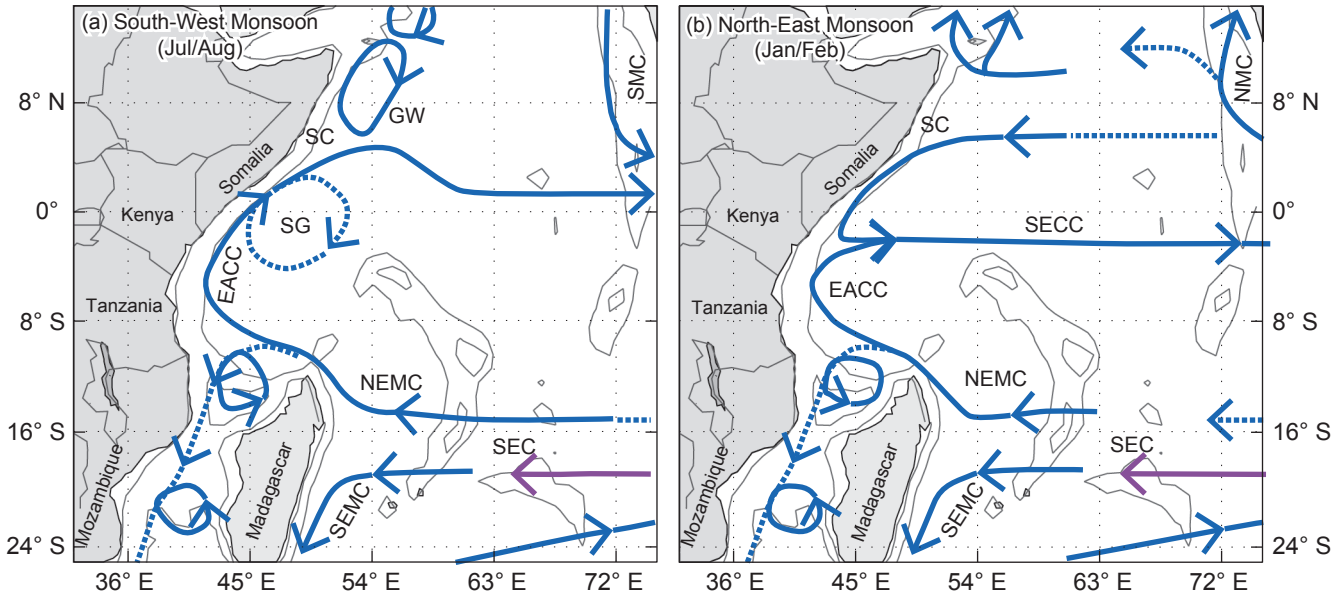

Figure 2: Schematic diagram of near-surface circulations in the tropical western Indian Ocean (in blue) and the subsurface return flow of the supergyre (in magenta) during (a) the South-West Monsoon and (b) the North-East Monsoon, adapted from Schott et al. (2009). Currents are the South Equatorial Current (SEC), South Equatorial Counter Current (SECC), North-East and South-East Madagascar currents (NEMC and SEMC), East African Coastal Current (EACC), Somali Current (SC), Southern Gyre (SG), Great Whirl (GW), and South-West and North-East Monsoon currents (SMC and NMC). Reproduced from *African Journal of Marine Science* (2014) 36: 233–252, with permission of NISC (Pty) Ltd

forms as a result of very strong anticyclonic wind stress curl generated offshore from the Somali coast and causes another cold wedge at 10°–12° N (Schott and McCreary 2001). The Great Whirl is almost completely closed in the late South-West Monsoon season from August to September, and has very small exchanges with the offshore flow. Another smaller recurrent eddy known as the Socotra Gyre (or Eddy) is formed at about 12° N (Pickard and Emery 1990; Schott and McCreary 2001).

During the North-East Monsoon, the northern edge of the weakened SEC shifts southward from its location between 10° S and 20° S during the South-West Monsoon as the south-east trades do (Schott et al. 2009). The north-easterly winds channelled by the East African highlands drive the southward-flowing Somali Current (also known as the Somali Counter Current). The southward limit can reach to 4° S before it turns offshore, where the north-easterly winds are stronger (Johnson et al. 1982). The north-easterly winds and the SC along the East African coast are in an opposite direction to the EACC during this period. As a result, the EACC is weakened to <0.2 m s^{-1} during November through March (Newell 1957; Dubi 2000; Julius 2005). Its weakest velocities are reported in February (Tomczak and Godfrey 1994), when the North-East Monsoon is fully developed. The surface ocean circulation in the tropical Indian Ocean during this monsoon is portrayed in Figure 2b. The northward-flowing EACC and the southward-flowing SC meet in a confluence zone ranging between 2° and 4° S during the North-East Monsoon (Swallow et al. 1991; Schott et al. 2009), resulting in an eastward offshore flow between 2° and 4° S known as the South Equatorial Counter Current (SECC) (Düing and Schott 1978; Schott and McCreary 2001). Kabanova (1968) suggested that when the SECC flows offshore from the coast, it may cause slight upwelling off the northern Kenyan coast. The SECC is attributed to the merging of the westward-flowing currents near the Seychelles–Chagos thermocline ridge (SCTR) (Hermes and Reason 2008; Yokoi et al. 2008). The SECC does not extend much beyond 70° E in January, being opposed in the east by a weak westward flow. It is best developed in February when it forms a continuous band across the Indian Ocean, causing high sea levels in the east (Morrow and Birol 1998). The velocities of the SECC are between 0.5 and 0.8 m s^{-1} in the west but weaker in the east. The current is masked by overlying westward Ekman currents during the South-West Monsoon (McCreary et al. 1993; Song et al. 2004; Schott et al. 2009).

During the monsoon transition periods (April/May and October/November), the Indian Ocean equatorial region experiences eastward-flowing equatorial currents driven by the relatively strong westerly winds along the equator that produce Ekman convergence there (McPhaden et al. 2009). These are the strong eastward surface jets, estimated to be about 1 m s^{-1} (Schott and McCreary 2001) and they differentiate the Indian Ocean from Pacific and Atlantic oceans. First identified by Wyrtki (1973), they are known as the Wyrtki jets. Models forced with two different realistic wind datasets by Anderson et al. (1993), Jensen (2003) and Han et al. (1999) showed that the Wyrtki jets are weaker in austral autumn than in spring.

Although there have been a number of model studies of the broader Indian Ocean, there has been no in-depth numerical study of the mean state and seasonal cycle of the upper ocean in the tropical western Indian Ocean, and specifically in the Tanzanian shelf region. Thus, this paper aims to understand better the annual mean state and

annual cycle of the circulation and dynamics in the western tropical Indian Ocean. It provides a detailed assessment of the annual cycle in the region beyond the brief discussion of this aspect in Manyilizu et al. (2014).

Using the Regional Ocean Modeling System (ROMS), the study addresses the following questions: (i) how do the upper-ocean dynamics vary throughout the year in the tropical western Indian Ocean; (ii) is the seasonality of the NEMC in phase with the EACC in the Tanzanian shelf region; (iii) how does advection from the NEMC influence the heat content of the upper ocean in Tanzanian shelf waters; and (iv) how does advection from the NEMC influence the salinity of the upper ocean in Tanzanian shelf waters?

Datasets and methods

The Regional Ocean Modeling System has been shown to simulate realistically the tropical Indian Ocean (Hermes and Reason 2008), the south-western Indian Ocean (Penven et al. 2006), the tropical western Indian Ocean (Manyilizu et al. 2014), the Comoros Basin (Collins et al. 2014) and the Zanzibar Channel (Mayorga-Adame et al. 2016). Thus, it is an established numerical tool for modelling ocean circulation in this region. The model is a free-surface, terrain-following ocean model that solves the three-dimensional hydrostatic primitive equations (Shchepetkin and McWilliams 2003, 2005). The vertical structure is discretised in stretched, terrain-following coordinates, and orthogonal curvilinear coordinates are applied in the horizontal structure on a staggered Arakawa C-grid. The K-profile parameterisation provides the model vertical mixing (Large et al. 1994). This research uses the Institut de Recherche pour le Développement (IRD) version of the code (ROMS AGRIF), available from http://www.romsagrif.org (Debreu et al. 2012).

The study adapted the model configuration used in Manyilizu et al. (2014), which was configured in the tropical western Indian Ocean for the domain 37.5°–60° E and 4.85° N–18° S with its bathymetry derived from ETOPO2V2C (see www.ngdc.noaa.gov; Figure 1). The model used a global topography dataset at 2′ resolution processed by Smith and Sandwell (1997). This run was an interannual simulation, forced from 1978 to 2007 by the National Centers for Environmental Prediction (NCEP) reanalysis-2 of winds and heat fluxes with two years' spin-up time. The NCEP 6-hourly reanalysis data with a linear temporal interpolation were applied through bulk formulae to derive the wind stresses and heat fluxes used throughout the model simulations. In this model configuration, the initial and lateral boundary conditions were extracted from the Simple Ocean Data Assimilation (SODA) 2.0.2-4 (Carton and Giese 2008). The monthly values were used to force the lateral open boundaries by means of linear temporal interpolation. The lateral boundary conditions were based on a combination of active adaptive radiation conditions added to nudging (reaching a nudging time-scale of 360 days) and sponge (reaching a viscosity/diffusivity value of 1 000 $m^2\ s^{-1}$) layers 150-km wide (Marchesiello et al. 2001). The model simulation had 40 vertical levels, ⅙° horizontal resolution and time-steps of 1 800 s. The model outputs were averaged every two model-days, which in turn were processed to calculate monthly and climatological data. In this experiment, no explicit restoring towards observed sea surface temperature (SST) was used in the bulk formula for the surface heat flux and the model was named Model_NCEP.

The model outputs from Model_NCEP were validated by another model configuration with different forcing over the same domain. With the same vertical levels, horizontal resolution and time-steps, the second model run was forced with the monthly mean Comprehensive Ocean and Atmosphere Data Sets (COADS) winds and heat fluxes (da Silva et al. 1994) for 10 years with a three-year spin-up time. The initial and lateral boundary conditions for this simulation were extracted from the World Ocean Atlas 2001 global dataset with monthly climatology 1° resolution (WOA2001; Conkright et al. 2002). A heat flux correction resulting in a restoring term on surface temperature was applied in this experiment and the run was termed Model_COADS.

In addition to observations, further validation was provided by the altimeter sea-surface height observations from Archiving, Validation and Interpretation of Satellite Oceanographic (AVISO) obtained from 1992 to 2007 at ⅓° resolution (www.aviso.oceanobs.com). These are gridded data that combine altimeter measurements from different satellites using an interpolation mapping technique (Ducet et al. 2000). Gridded maps of absolute dynamic topography (MADT) were used in comparisons with the model. Owing to different absolute values of sea surface height (SSH) in ROMS and AVISO due to their different reference levels, the spatial SSH deviations from their spatial mean are represented here.

Wind stress, τ, was approximated by:

$$\tau = (\tau_x, \tau_y) = \rho_a C_d |W|(u, v)$$

where τ_x and τ_y are the zonal and meridional wind stress components, respectively. Air density, ρ_a, is taken as 1.225 kg m^{-3}, C_d is the drag coefficient and W is the magnitude (wind speed) of the zonal (u) and meridional (v) components of the wind. The value of C_d is dependent on atmospheric stability and wind speed.

Wind stress curl plays a significant dynamical role as a source of vorticity in the upper-ocean surface. It is directly related to the Sverdrup balance for the volume transport. The z component of the wind stress curl vector is given by the following equation:

$$\mathrm{Curl}_z\tau = \frac{\partial \tau^y}{\partial x} - \frac{\partial \tau^x}{\partial y}$$

where positive (negative) wind stress curl in the Northern Hemisphere is cyclonic (anticyclonic) and in the Southern Hemisphere is anticyclonic (cyclonic).

Ekman pumping is generated by the wind stress curl as an open-ocean upwelling and downwelling (Risien and Chelton 2008). It is associated with Ekman velocities, which are caused by frictional forces. Therefore, the Ekman pumping velocities are expressed as a function of the applied wind stress, as follows:

$$W_e = \frac{1}{\rho f}\left(\frac{\partial \tau^y}{\partial x} - \frac{\partial \tau^x}{\partial y}\right) = \frac{1}{\rho f}\mathrm{Curl}_z\tau$$

where W_e is the vertical Ekman velocity, ρ is the density of sea water, f is the Coriolis parameter, $f = 2\,\Omega \sin(\theta)$ where $\Omega = 7.29 \times 10^{-5}$ s^{-1}, and θ is latitude. The Ekman pumping equation is not applied within about 2° of the equator where f goes to zero. The upward (downward) vertical velocities due to the applied wind stress are usually referred to as Ekman suction (pumping) velocities.

Results

Mean state

Figure 3 shows the mean state of the wind stress, wind stress curl and vertical Ekman velocity in the tropical western Indian Ocean for the NCEP and COADS configurations. Wide bands of negative and positive wind stress curl, as suggested by Collins et al. (2012), appear in both datasets. There is a strong spatial gradient between the anticyclonic and cyclonic wind stress curl between the area north-east of Madagascar and that to the north and north-west, extending in a band towards Tanzania (Figure 3a, b). The band of the anticyclonic wind stress curl extending from Madagascar towards Tanzania is narrower in the COADS data but stronger in magnitude just to the north-west of Madagascar. This band is associated with generally equatorward wind stress in this area (Figure 3a, b). The anticyclonic wind stress curl in this band results in Ekman convergence and, consequently, downwelling in the region (Figure 3c, d). To the north-east of Madagascar there is cyclonic (negative) wind stress curl, which can be associated with strong south-easterly trade wind stress. As a result, weak upwelling occurs both north and south of the equator. The negative curl north-east of Madagascar is important for the formation of the SCTR (Hermes and Reason 2008).

The mean spatial distributions of the annually averaged surface current speeds from the model were compared to geostrophic currents estimated from the AVISO satellite data. In the model simulations and the AVISO data, strong currents occur along the East African coast and to the north of Madagascar, reflecting the EACC and the NEMC, respectively (Figure 4, top panel). The NEMC, which flows north-westward past the north of Madagascar, has speeds ranging from 60 to 70 cm s^{-1}, in agreement with the observed 70 cm s^{-1} reported by Schott and McCreary (2001). The NEMC bifurcates near the African coast between 10° and 12° S into the northward-flowing EACC and a southward flow into the Mozambique Channel. The EACC shows the strongest annual average current speeds between 8° S and the equator (ranging from 100 to 120 cm s^{-1}) in both the model and the satellite-derived data.

The tropical western Indian Ocean indicates contrasting north–south SSH patterns in the mean state for the model and AVISO. High SSH appears south of 10° S and along the East African coast in the ROMS simulations and the AVISO data (Figure 4, bottom row). The lowest surface height appears around 8° S in the tropical western Indian Ocean between the SEC and SECC (Donguy and Meyers 1995).

The mean volume transport integrated in the upper 1 500 m in the tropical western Indian Ocean from the model is shown in Figure 5. A volume transport of up to 35 Sv and 25 Sv occurs to the north of Madagascar for Model_NCEP and Model_COADS, respectively. These annual mean values to the north of Madagascar reflect the NEMC, agreeing reasonably well with the value of 29.60 Sv reported by Swallow et al. (1988) and Schott et al. (2009). The annual mean volume transported by the EACC appears to be about 20 Sv in Model_NCEP and 25 Sv in Model_COADS. The EACC is the western boundary current of a cyclonic tropical gyre, which comprises the SEC to the south and the South Equatorial Counter Current in the north during the North-East Monsoon season and the Wyrtki jets in the transition seasons. However, during the South-West Monsoon season, the northern branch of this gyre lies north of the equator. The mean volume transport in the two model runs (Figure 5) indicates differences in the central basin, suggesting that the volume transport in the region is sensitive to different forcing. These discrepancies could be due to differences in the spatial and temporal resolutions and the boundary conditions for Model_NCEP and Model_COADS.

Summarising, there are a few differences in the annual mean model currents and volume transports in the tropical western Indian Ocean, consistent with the differences in wind stress curl (Figure 3). In general, the Tanzanian shelf region experiences anticyclonic wind stress curl, leading to Ekman convergence and downwelling. Furthermore, the Tanzanian coastal waters are dominated by the EACC, which reflects high SSH and volume transport.

Annual cycle

The annual cycles of Model_NCEP and Model_COADS were assessed in conjunction with the AVISO data. Since the tropical western Indian Ocean experiences strong seasonality, it is useful to discuss its annual cycle starting with May, the monsoon transition season, then July, midway through the South-West Monsoon, followed by November (monsoon transition) and then January, midway through the North-East Monsoon season.

Wind stress, wind stress curl and Ekman pumping

The annual cycle of the upper-ocean dynamics in the tropical western Indian Ocean was examined first through the wind stress, wind stress curl and Ekman pumping (Figures 6, 7).

In May, a contrast in wind stress curl occurs between the anticyclonic curl in the west and south of the domain and cyclonic curl elsewhere in the domain, except in the Mozambique Channel (Figure 6a, b). Strong, positive (anticyclonic) wind stress curl is confined to the north-west of Madagascar and extends towards the Tanzanian coast. The strong wind stress curl reflects the relatively strong equatorward wind stress (Figure 6a, b). This anticyclonic wind stress curl results in Ekman convergence and consequently downwelling along the Tanzanian coast to the south of 5° S in the NCEP run but less obviously in COADS (Figure 7a, b). The rest of the tropical western Indian Ocean is dominated by weak, negative wind stress curl, which leads to upwelling. Similar spatial patterns of the wind stress curl and Ekman

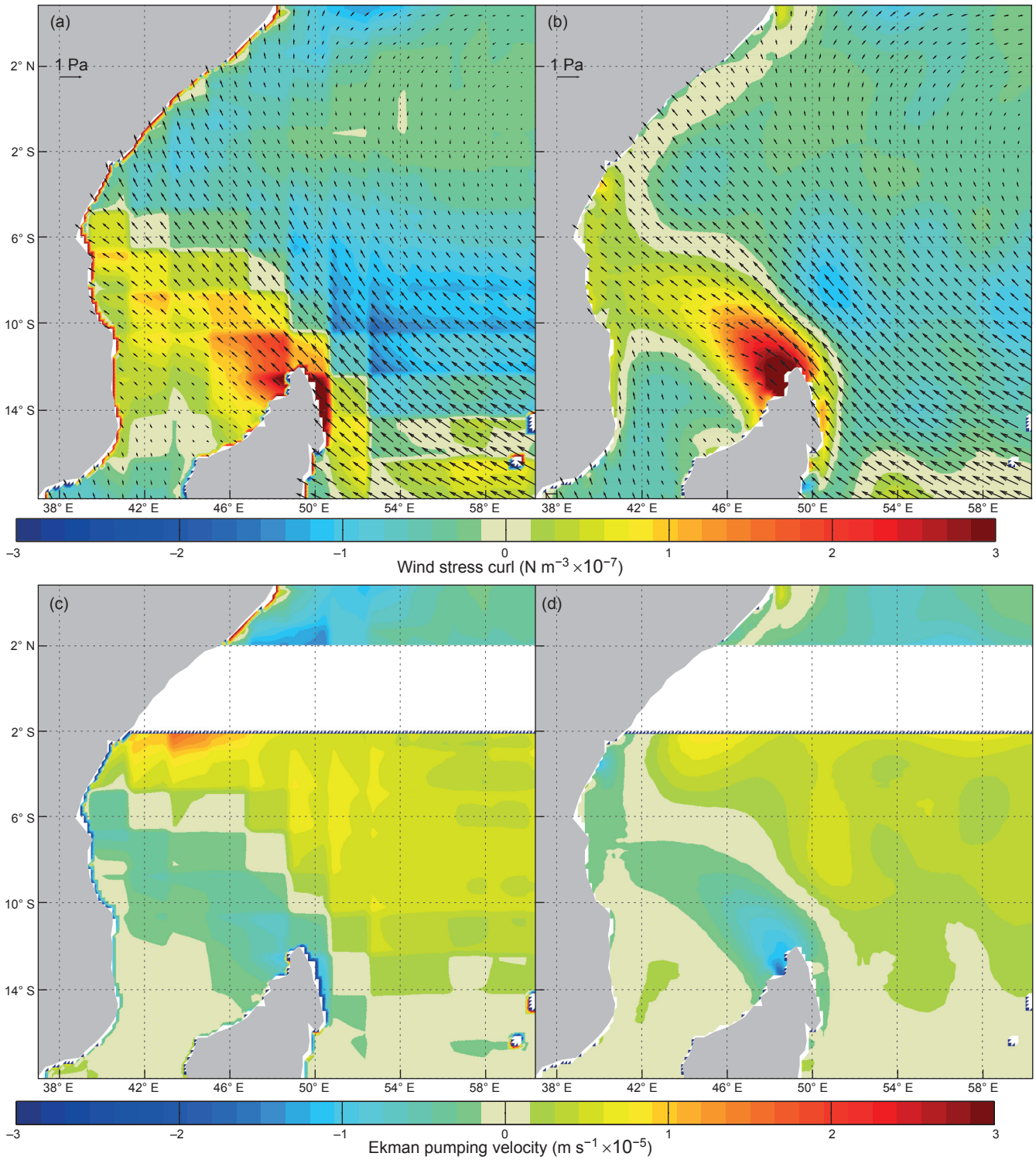

Figure 3: (a, b) Annual mean of wind stress (vectors) and its corresponding wind stress curl (in colour) and (c, d) Ekman pumping velocity over the tropical western Indian Ocean for the Model_NCEP run (left column) and the Model_COADS configuration (right column)

pumping occur in July, but they become stronger than in May due to enhanced wind stress that feeds into the South-West Monsoon (Figure 6c, d). During July, the downwelling patterns observed in May extend to the Tanzanian coast in both model simulations (Figure 7c, d).

Different spatial distributions of the wind stress, wind stress curl and Ekman pumping occur during the period of transition to the North-East Monsoon as well as the monsoon season itself (October–March). In November, the wind stress curl is weakened, with the zone of negative

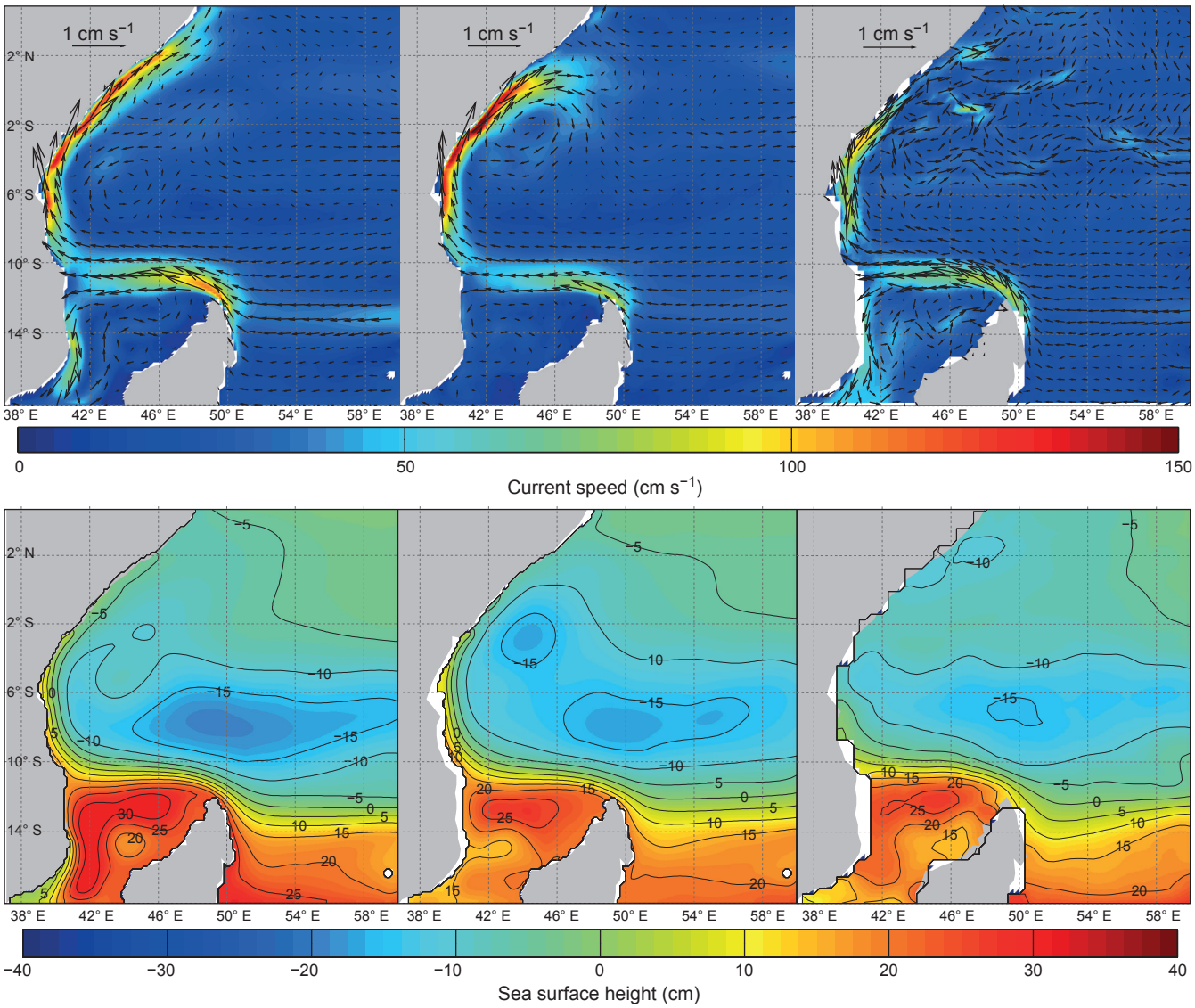

Figure 4: Annual mean of surface current speeds superimposed on the surface current speed (top row) and sea surface height (bottom row) in the tropical western Indian Ocean, extracted from the ROMS model forced with Model_NCEP (left column) and Model_COADS (middle column), and from MADT_AVISO data (right column)

wind stress curl confined to between 2° and 6° S near the coast and to between 2° and 14° S in the east (Figure 6e, f). Relatively weak anticyclonic curl occurs to both the north and south of this band with strong values just to the north of Madagascar and extending towards Tanzania. As a result, downwelling occurs in this band from northern Madagascar towards and along the Tanzanian coast to about 6° S in November (Figure 7e, f). In January, most of the domain is characterised by positive wind stress curl and strong wind stress, except to the east and north-east of Madagascar, part of the northern Mozambique Channel and in an alongshore band offshore from the Kenyan and Somali coasts (Figure 6g, h). During this period, the downwelling that occurs to the north of Madagascar and extends towards Tanzania now reaches 2° S as well as eastwards across most of the domain in the 2–8° S band (Figure 7g, h).

Sea surface height, currents and volume transport

Figures 8–9 show the annual cycle of the surface currents and SSH over the domain in the model and AVISO, Figure 10 the seasonal SSH variance and Figure 11 the model volume transport. For Model_NCEP, the EACC is in phase with the NEMC throughout the year with volume transport peaking in June through July (Figure 11a). The currents are correlated at about 0.7 (significant at the 95% level) when the NEMC lags behind the EACC by two to three months in both model simulations. Although the patterns of the volume transported in both models are similar, the volume for the Model_COADS run appears to be less than that for the Model_NCEP run for most of the year. This difference may result from differences in the wind forcing in the two datasets. The annual cycle of the SSH (Figure 9) indicates a north–south distribution in the region with seasonal variation in both model simulations and AVISO. High SSH

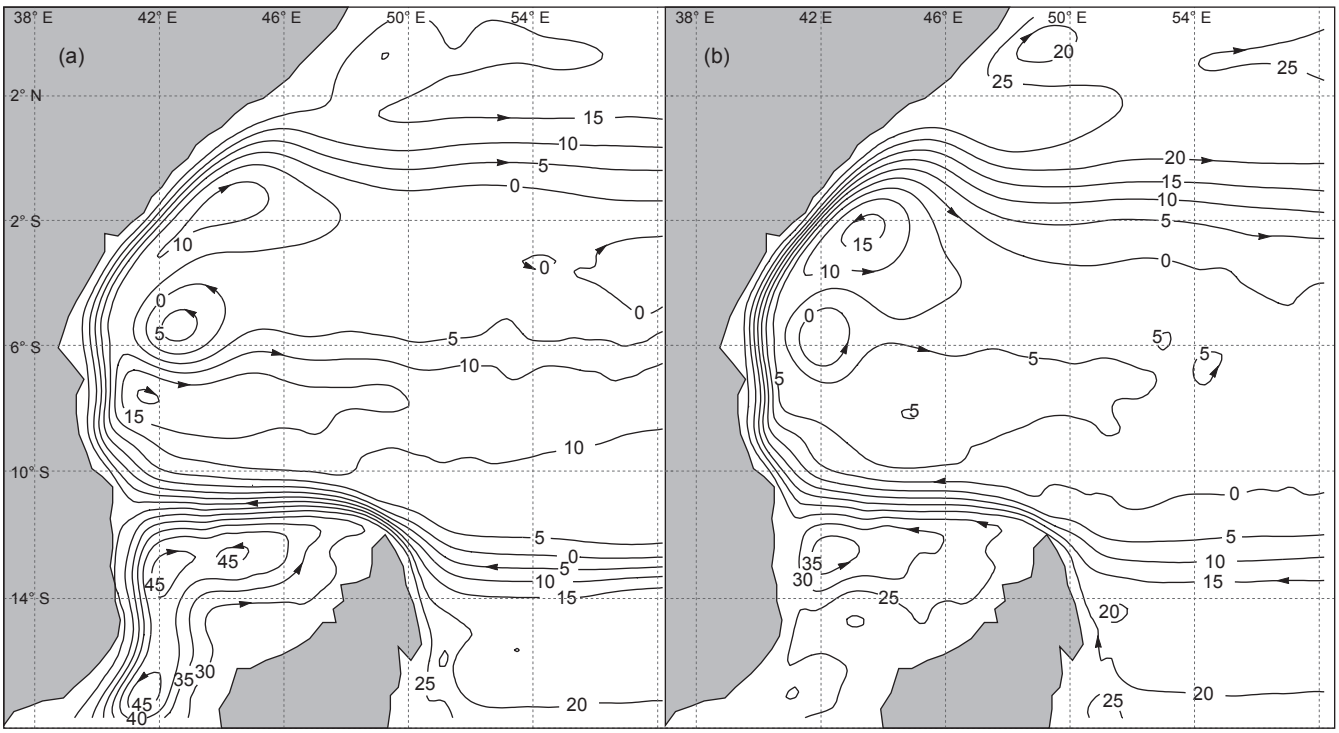

Figure 5: Annual mean upper-ocean volume transport (Sv) integrated from the surface to 1 500 m for (a) Model_NCEP and (b) Model_COADS

occurs to the south of 10° S and along the Tanzanian coast during all months. The SSH difference between high and low sea levels in the domain is higher than 40 cm. The SSH variance in Model_COADS seems to be higher than that of Model_NCEP and AVISO, suggesting that the NCEP run is better than COADS. Such differences can be associated with differences in spatial and temporal resolutions of the forcings and lateral boundary conditions. Minimum SSH variance (<5 cm^2) occurs on the Tanzanian shelf, extending offshore towards the centre of the domain in the model simulations and AVISO data (Figure 10). However, high SSH variance occurs in the Mozambique Channel, north-east of Madagascar and to the north, centred around 44° E and 2° S, extending towards the north of the domain.

During the transition (May) to the South-West Monsoon, both the model and satellite data show near-surface currents and SSH in the tropical western Indian Ocean, which reflect the basin-wide cyclonic tropical gyre. This gyre comprises the SEC and the NEMC to the south, the EACC to the west and the eastward-flowing Wyrtki jets to the north (Figure 8a). They appear in the surface currents between 2° N and 2° S, and are strong and clearly visible in the open ocean to the east of 54° E. Patterns of high SSH in the model and AVISO align with the SEC and the NEMC to the south, the EACC to the west and the eastward-flowing Wyrtki jets to the north (Figure 9a). The most negative (cyclonic) SSH values in the model and the AVISO data extend from southern Tanzanian waters eastwards to the open ocean between 5° S and 12° S. This region of cyclonic values is elongated and centred at 8° S, 52° E in the model and farther east in the AVISO data. During this period, the NEMC flows strongly from the northern tip of Madagascar north-westwards towards the Tanzanian shelf (about 100 cm s^{-1}). The NEMC supplies the northward-flowing EACC near the African coast with speeds that reach up to 120 cm s^{-1}. The volume transported into the southern Tanzanian shelf region by the NEMC increases from c. 45.0 Sv in April to 47.2 Sv in May in Model_NCEP but only increases slightly in Model_COADS (Figure 11).

By the time the South-West Monsoon peaks in July, the tropical western Indian Ocean shows the strongest seasonal near-surface current speeds, SSH gradients and volume transport in both model and AVISO (Figures 8b, 9b, 11). The SEC and the NEMC appear to be located farther north in July than in May in their supply of the EACC, as suggested by Schott et al. (2009). The speeds of the EACC can be greater than 150 cm s^{-1} in July, feeding the northward-flowing SC. After crossing the equator, part of the SC turns offshore to the east where it recirculates, forming the Southern Gyre between 1° N and 6° S. The Southern Gyre, which is completely closed, appears to extend too far northward and southward in Model_NCEP and Model_COADS, respectively. High SSH patterns in Model_NCEP, Model_COADS and AVISO, which align with the SEC and the NEMC to the south as well as with the EACC to the west, are maintained. The most negative SSH values occur between 5° and 12° S and are centred at 8° S, 50° E in Model_NCEP and farther west in Model_COADS and AVISO. The westward (negative) volume transport in the NEMC north of Madagascar peaks in June and July at about 52.3 Sv in Model_NCEP, followed by weaker volume transport of about 43 Sv in August and September (Figure 11a). Subsequently, the volume transported alongshore on the Tanzanian shelf in the EACC peaks in June at about

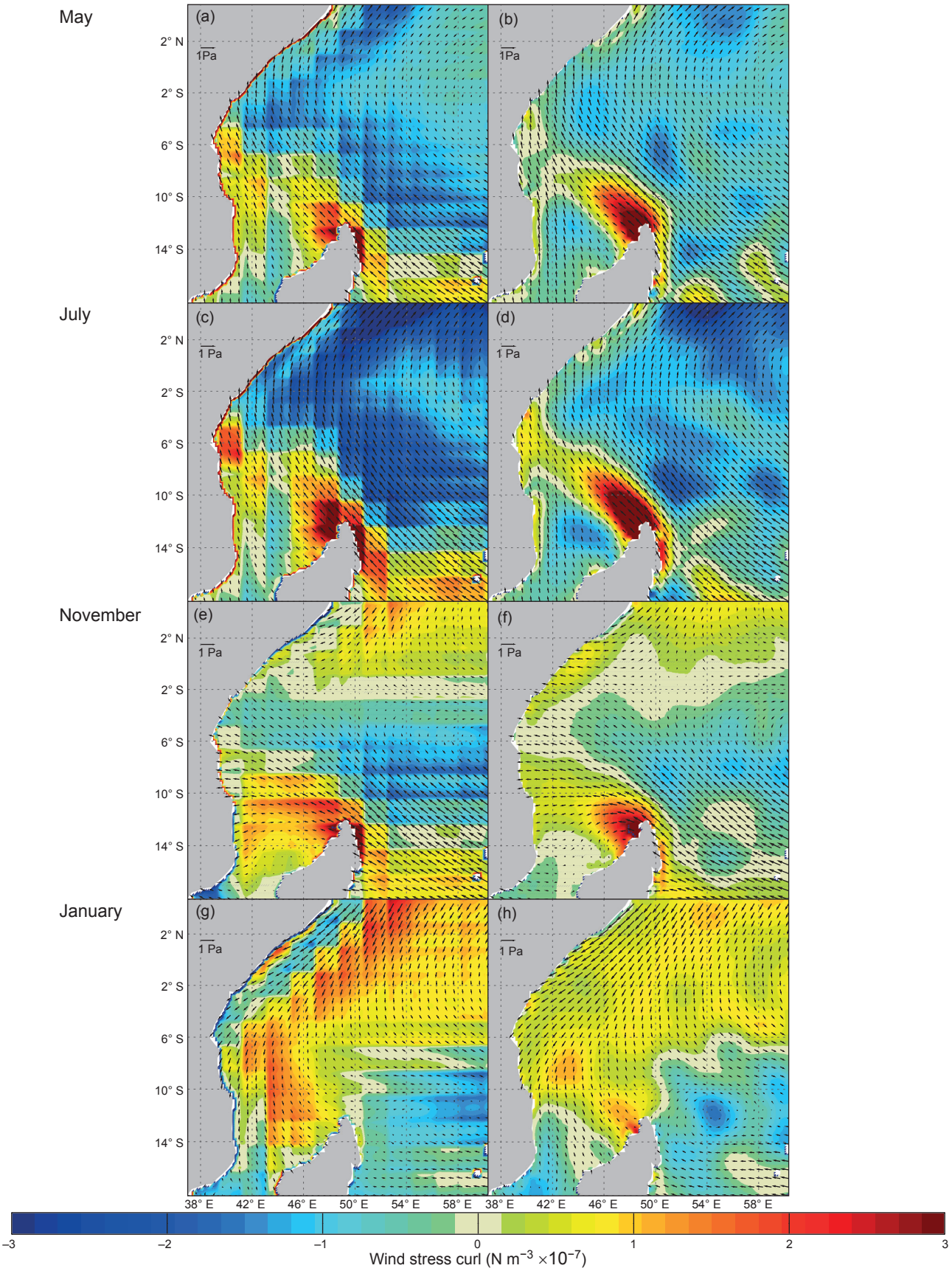

Figure 6: Annual cycle of wind stress (vectors) and its corresponding wind stress curl (in colour) over the tropical western Indian Ocean for Model_NCEP (left column) and the Model_COADS (right column) for (a, b) May, (c, d) July, (e, f) November and (g, h) January

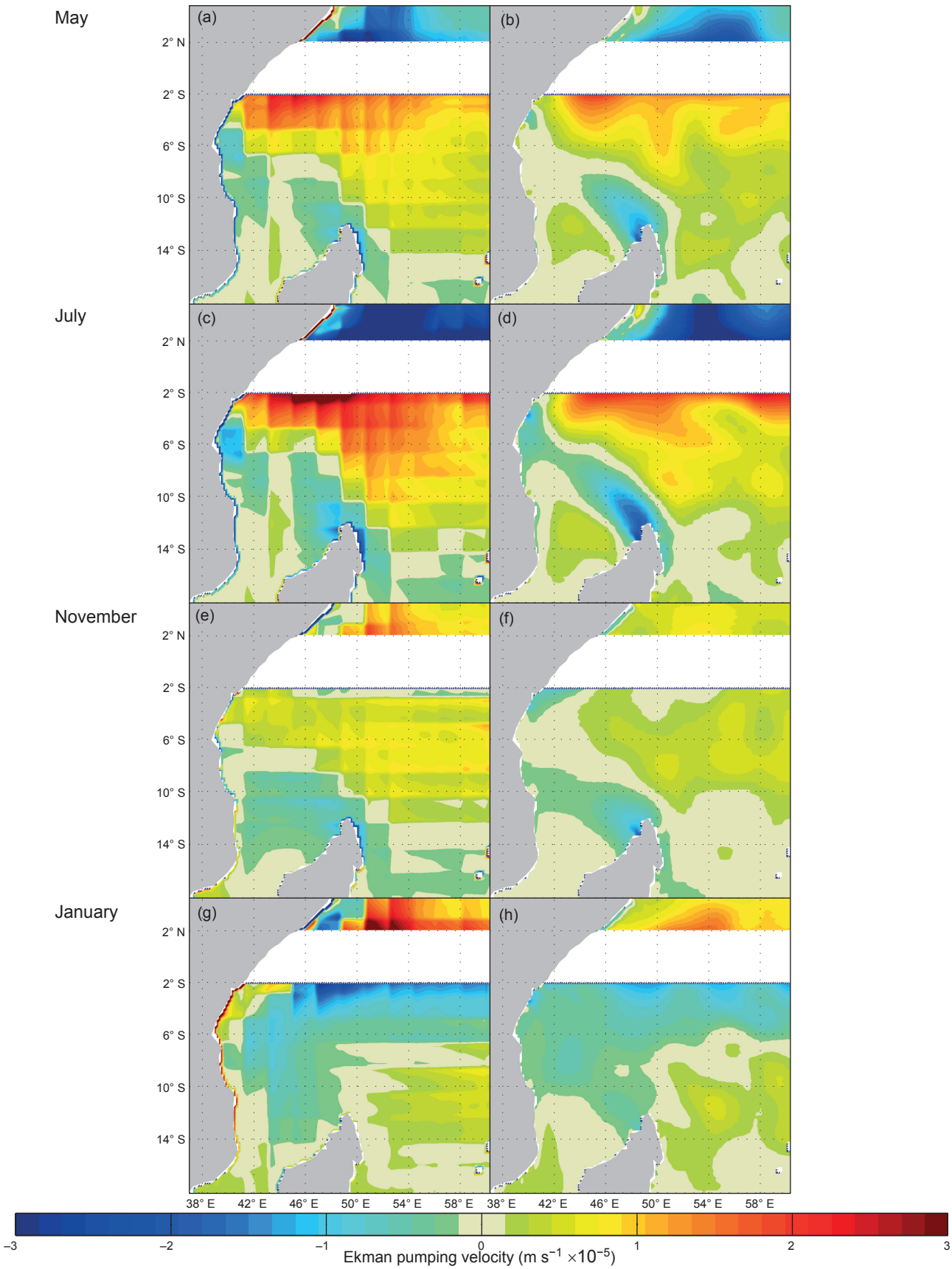

Figure 7: Annual cycle of Ekman pumping velocity over the tropical western Indian Ocean for Model_NCEP (left column) and Model_COADS (right column) for (a, b) May, (c, d) July, (e, f) November and (g, h) January

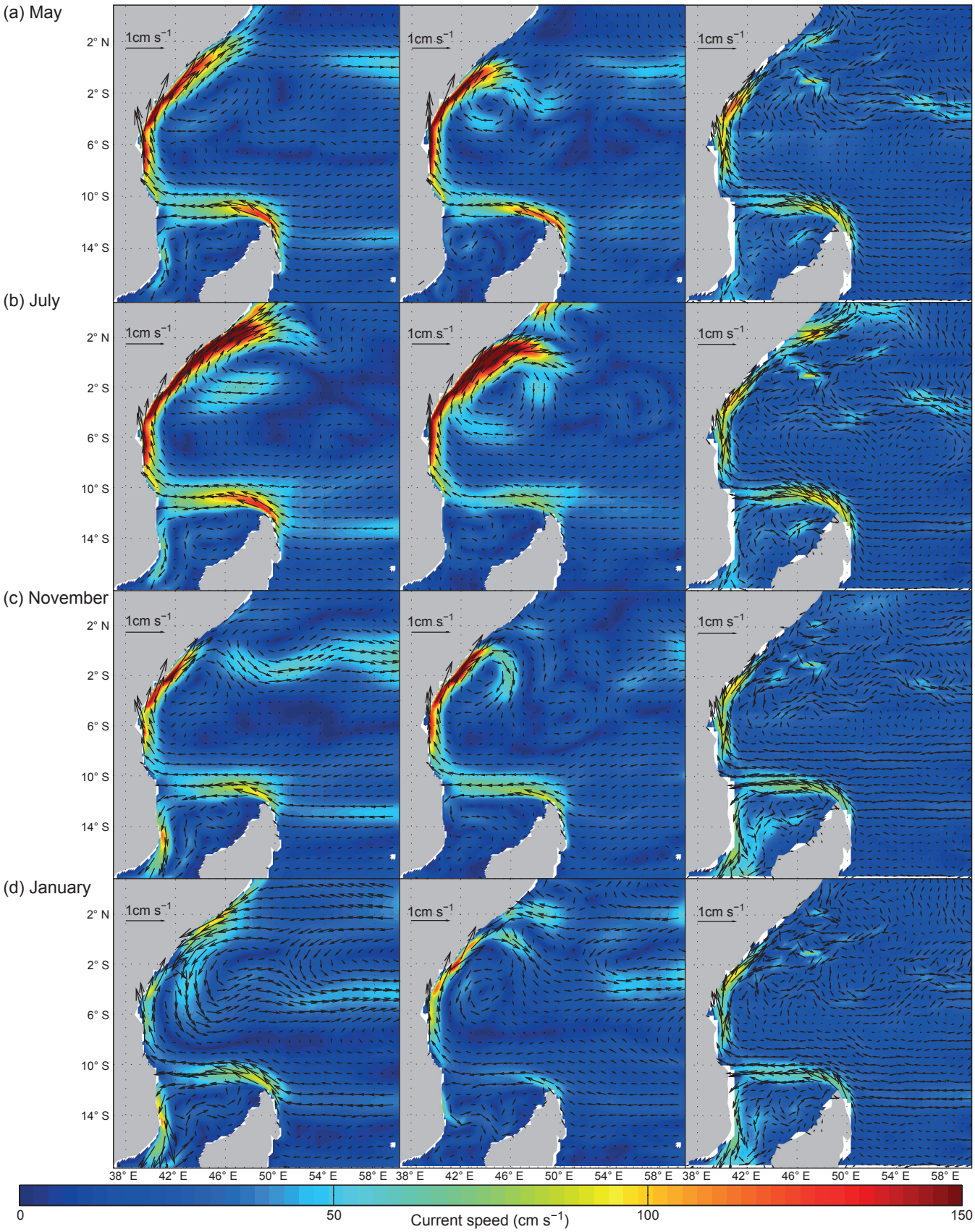

Figure 8: Annual cycle of surface current components superimposed on the surface current in the tropical western Indian Ocean for Model_NCEP (left column), Model_COADS (middle column), and MADT_AVISO (right column) in (a) May, (b) July, (c) November and (d) January

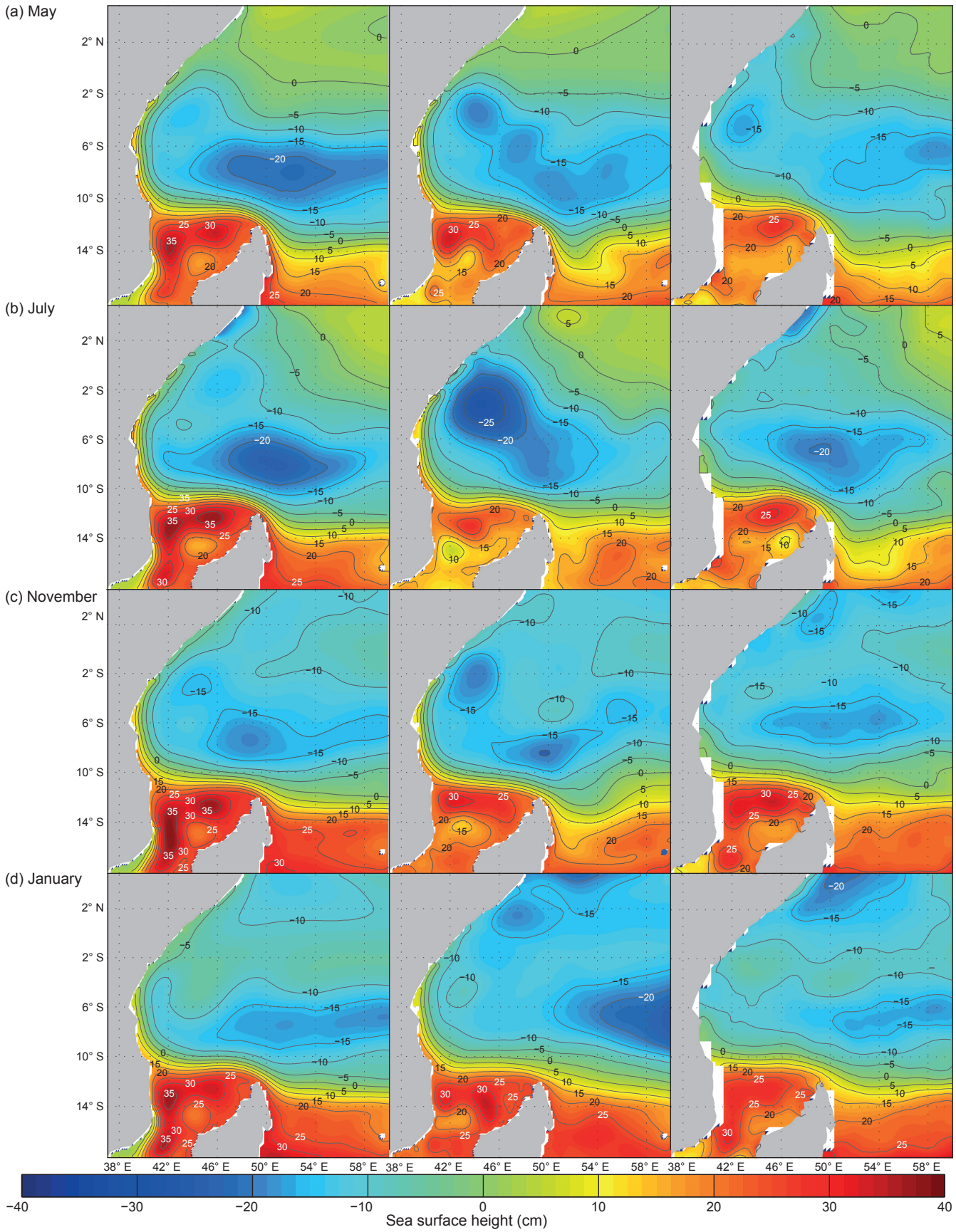

Figure 9: Annual cycle of sea surface height in the tropical western Indian Ocean for Model_NCEP (left column), Model_COADS (middle column), and MADT_AVISO (right column) in (a) May, (b) July, (c) November and (d) January

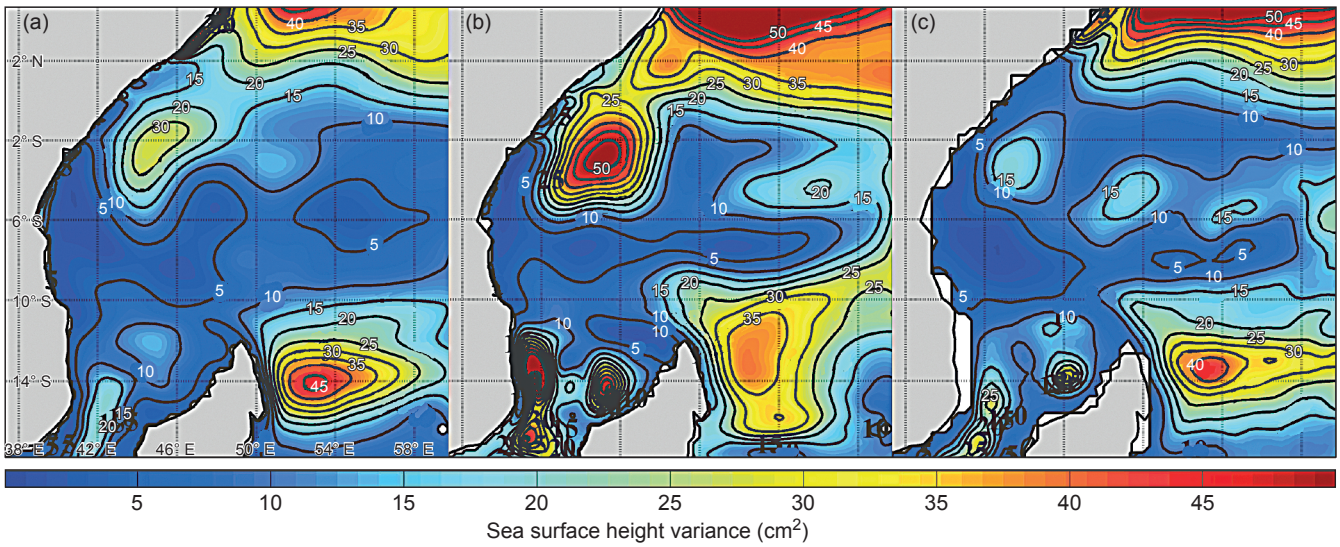

Figure 10: Seasonal variance of the sea surface height in the tropical western Indian Ocean extracted from the ROMS model forced with (a) Model_NCEP and (b) Model_COADS, and (c) from MADT_AVISO data

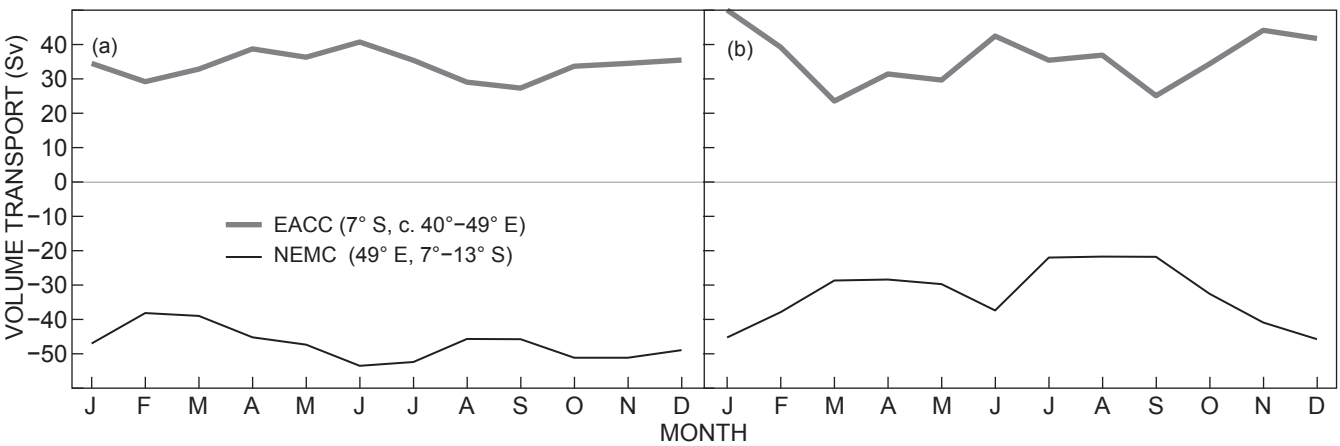

Figure 11: Climatology of the volume transport integrated between the surface and 1 500 m for the NEMC to the north of Madagascar and for the EACC in the southern Tanzanian shelf region for (a) Model_NCEP and (b) Model_COADS. Negative values indicate westward transport; positive values indicate northward and eastward transport

40 Sv, followed by weaker volume transport of about 28–30 Sv in August and September (Figure 11).

During the transition period (November) to the North-East Monsoon, the surface currents and SSH continue to reflect the basin-wide cyclonic tropical gyre. As in May, the gyre is bounded by the SEC and the NEMC to the south, the EACC to the west and the Wyrtki jets to the north in the model and AVISO (Figures 8c, 9c). The near-surface currents in the region are weaker than in July due to the weak winds blowing over the region. The Wyrtki jets tend to be stronger in November (about 80 cm s^{-1}) than in May (50–60 cm s^{-1}), as suggested by Han et al. (1999). The SEC and the NEMC are now located farther south with flow that feeds the EACC that is weaker than in July. The EACC has speeds ranging between 80 and 120 cm s^{-1}. High SSH patterns in the model simulations and AVISO align with the SEC and the NEMC to the south, the EACC to the west and the eastward-flowing Wyrtki jets to the north. The westward volume transport across the north of Madagascar is about 50 Sv in October and November and a moderate volume (about 35 Sv) is transported alongshore on the Tanzanian shelf during October and November (Figure 11).

During January, when the North-East Monsoon is fully developed, relatively weak surface ocean currents, SSH gradients and volume transport occur in the region in both models and AVISO. During this period, a reversal in the SC occurs to the north of 2° S, and the EACC is weakened to the south of 2° S in both model experiments and AVISO (Figure 8d). This flow pattern is attributed to the north-easterly winds that blow towards and along the East African coast and that drive the southward-flowing SC that crosses the equator. This current merges with the EACC between 1° S and 4° S, forming the SECC, which is clearly visible to the east of 54° E in the model results and AVISO (Figure 8d).

The SEC, the NEMC and the EACC are relatively weak in January with respective current speeds <40 cm s^{-1}, about 70 cm s^{-1} near the tip of Madagascar, and <50 cm s^{-1} along the East African coast. This relatively weak flow is attributed to the southward-flowing SC and the north-easterly winds that oppose the NEMC and the EACC. During this period, the SECC forms the northern boundary of the tropical gyre, which is located farther south than in the transition periods. High SSH values in the model and AVISO align with the SEC and the NEMC to the south, the EACC to the west and the eastward SECC to the north. The most negative SSH values in the model and AVISO occur in a band north and north-east of Madagascar between 5° and 10° S. The westward volume transport in the NEMC across the north of Madagascar decreases to a minimum value of about 38 Sv in February and March, as the northward volume transport in the EACC on the Tanzanian shelf decreases to its minimum value of about 30–33 Sv in the same months (Figure 11).

Impacts of the upper-ocean dynamics on the upper temperature and salinity

Here, time-series of volume transports in the EACC and NEMC, as well as a meridional transect north of Madagascar and a zonal transect in the middle Tanzanian shelf from Model_NCEP (Figures 12, 13), are analysed to assess the seasonal variability of temperature and salinity north of Madagascar and how the Tanzanian shelf responds seasonally to the flow north of Madagascar.

Figure 12 displays the vertical structure of the currents, temperature and salinity for a transect running from the northern tip of Madagascar at 13° S to 1° S, averaged between 49° and 49.5° E for each season. Common to all variables is a strong downward gradient near the north coast of Madagascar between 11° and 13° S throughout the year. For currents, this region indicates a core of intense westward flow, intensified at the surface, reflecting the westward-flowing NEMC (Figure 12a–d). Temperature and salinity show strong seasonal variability along the transect (Figure 12e–h and Figure 12i–l, respectively). Together with the wind stress and the surface heat fluxes over the region, these upper-ocean patterns suggest that the westward-flowing NEMC strongly influences the temperature and salinity distributions. As the isotherms and isohalines are vertically displaced downward (negatively sloped) towards the Madagascar coast, the NEMC is seen to transport warm and relatively fresh water westwards onto the Tanzanian shelf.

In May, before the onset of the South-West Monsoon, relatively strong currents occur between 11° and 13° S just to the north of Madagascar (Figure 12a). There, current speeds >70 cm s^{-1} occur in the upper 150 m, indicative of the NEMC. May is characterised by moderate winds that reduce the wind-induced evaporative heat loss and vertical mixing. As a result, warm surface temperatures of about 27–28 °C occur in the upper 50 m (Figure 12e). This temperature is favourable for convective rainfall leading to relatively fresh surface waters (<34.7 salinity) south of 8° S (Figure 12i). Such patterns occur with the eastward-flowing currents that reflect the Wyrtki jets near the equator, at around 5° S at 50 m depth. The model seems to show eastward flow in this region. The isotherms and isohalines below 50 m show downward slopes around 10° S with a strong westward NEMC (about 50 cm s^{-1} at 60 m depth). The deepening of the warm isotherms and fresh isohalines between 7° and 12° S suggests that the westward NEMC also plays a significant role here, possibly by either carrying warm and fresh waters or by interrupting the upwelling over the open ocean (Hermes and Reason 2008; Yokoi et al. 2008).

During July, when the South-West Monsoon is fully developed, the transect indicates greater current speeds near northern Madagascar than in May, with relatively cool and salty surface waters (Figure 12b, f, j). The zonal current speeds strengthen to more than 70 cm s^{-1} at 150 m depth between 11° and 12° S to the north of Madagascar, identifying the NEMC (Figure 12b). This region shows relatively cool and salty surface waters (c. 24–25 °C, c. 34.8–34.9) in the upper 75 m, with cool waters (c. 25 °C) lying adjacent to the northern coast of Madagascar. The zonal currents in the upper 250 m off the northern coast of Madagascar broaden from May to July and cool by about 2 °C (Figure 12b). This behaviour is due to the strong winds over the tropical western Indian Ocean that enhance both the wind-induced evaporative cooling and the vertical mixing. Moreover, there is increased cloud cover in July, reducing the solar insolation and thus decreasing the net surface heat flux gain and leading to further cooling of the surface temperature. There is a smaller temperature difference between the surface and subsurface waters in July. For example, the 20 °C isotherm is located at about 150 m depth in July, compared with about 140 m in May. The bottom doming of the isothermal and isohaline structures between 5° and 10° S is maintained, with a weakening in the gradients compared with those in May.

In November, the transition period to the North-East Monsoon, the transect indicates relatively weak currents and salty, warm surface waters with strong current speeds being confined to the subsurface waters (Figure 12c, g, k). The weakened currents near the northern coast of Madagascar reflect the NEMC. The upper surface temperature ranges between 26 and 27 °C in the upper 50 m depth, and the 27 °C isotherms of surface waters are largely confined to the south. The entire transect indicates high salinity that ranges between 34.8 and 35.1 from the surface to 250 m. Similar to May and July, the deepening of the warm isotherms and fresh isohalines appears between 11° and 13° S, suggesting that the westward NEMC plays a significant role in this process. This is possibly because the NEMC either carries warm salty waters towards the Tanzanian shelf or interrupts the flow of upwelled waters onto the northern Madagascar shelf from the SCTR that occurs throughout the year.

During January, when the North-East Monsoon is fully developed, relatively weak currents and warm fresh waters are evident towards the middle of the transect (Figure 12d, h, l). The NEMC appears in the region between 11° and 13° S and dominates the westward currents. The region is characterised by the upward displacement of the warm isotherms and salty isohalines towards the surface and off the northern tip of Madagascar. Such patterns can be associated with the westward NEMC by either carrying warm and

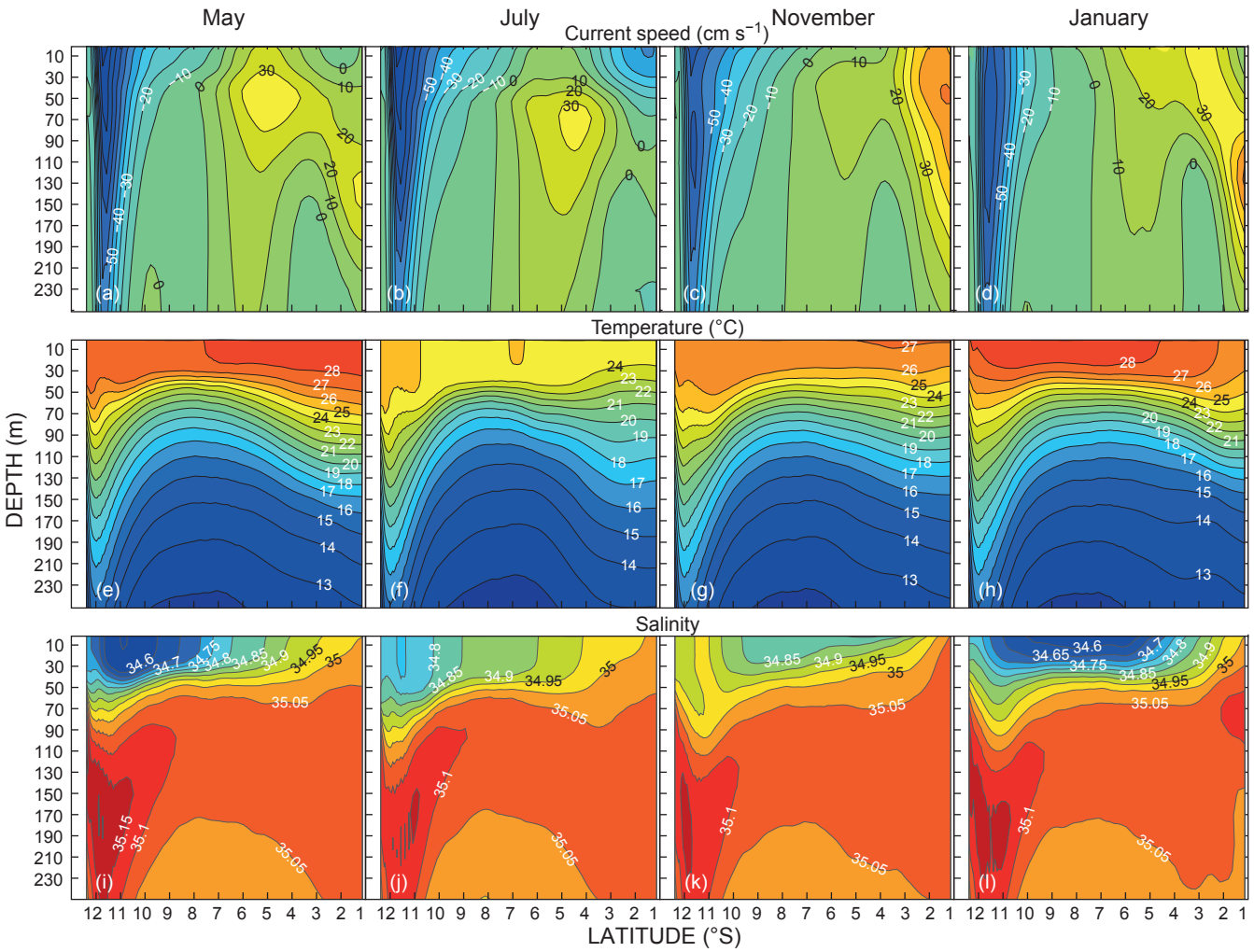

Figure 12: Vertical sections of (a–d) cross-shore current component (10 cm s^{-1} contour intervals), (e–h) temperature (1 °C contour intervals) and (i–l) salinity (0.05 contour intervals) averaged over 49–49.5° E from 1° S to 13° S for Model_NCEP

salty waters or by interrupting the flow of water upwelled onto the north Madagascar shelf from the open ocean region. Warm temperatures of about 28 °C and low salinity of about 34.7 that appear from the surface to a depth of about 40 m in the middle of the transect can be associated with the position of the intertropical convergence zone (ITCZ), which is at 12° S by the end of December. North of 8° S is dominated by an eastward flow that reflects the SECC.

Strong upper-ocean currents that influence the temperature and salinity distribution occur in the central Tanzanian shelf waters (Figure 13). The transect from the coast of Tanzania near 40° E to offshore at 49° E and averaged between 7° and 7.5° S indicates strong northward ocean currents with some seasonal variation across the mid-Tanzanian shelf region. The strong northward alongshore current speeds are confined to the Tanzanian coast and reflect the northward-flowing EACC. The seasonal variation of the EACC in the Tanzanian shelf region leads to variations in temperature and salinity in the upper 50 m with weaker changes below this depth.

The northward-flowing EACC influences the upper-ocean temperature and salinity during May (Figure 13a, e, i) and July (Figure 13b, f, j). In May, the surface waters in the upper 50 m are warmer than 27 °C and fresher than 34.6, with isotherms and isohalines being displaced vertically upward near the Tanzanian coast. This pattern is indicative of the equatorward-flowing EACC, which possibly influences the vertical temperature and salinity distributions by interrupting the weak downwelling flow of waters near the coast. In July, the 25 °C isotherm and 34.8 isohaline appear to be displaced vertically upward offshore and deepened near the coast in the upper 50 m. Such patterns suggest that the broadened northward-flowing EACC transports the cool and relatively high salinity waters northwards and interrupts the strong mixing and downwelling along the coast in May. This behaviour results from the strongest and steadiest southerly to south-westerly winds over the region in May leading to considerable downwelling along the Tanzanian shelf, and enhanced wind-induced evaporative cooling and vertical mixing and thus surface cooling.

November and January show relatively weaker ocean currents which influence the warm and salty waters near the coast (Figure 13c, g, k and Figure 13d, h, l, respectively). In

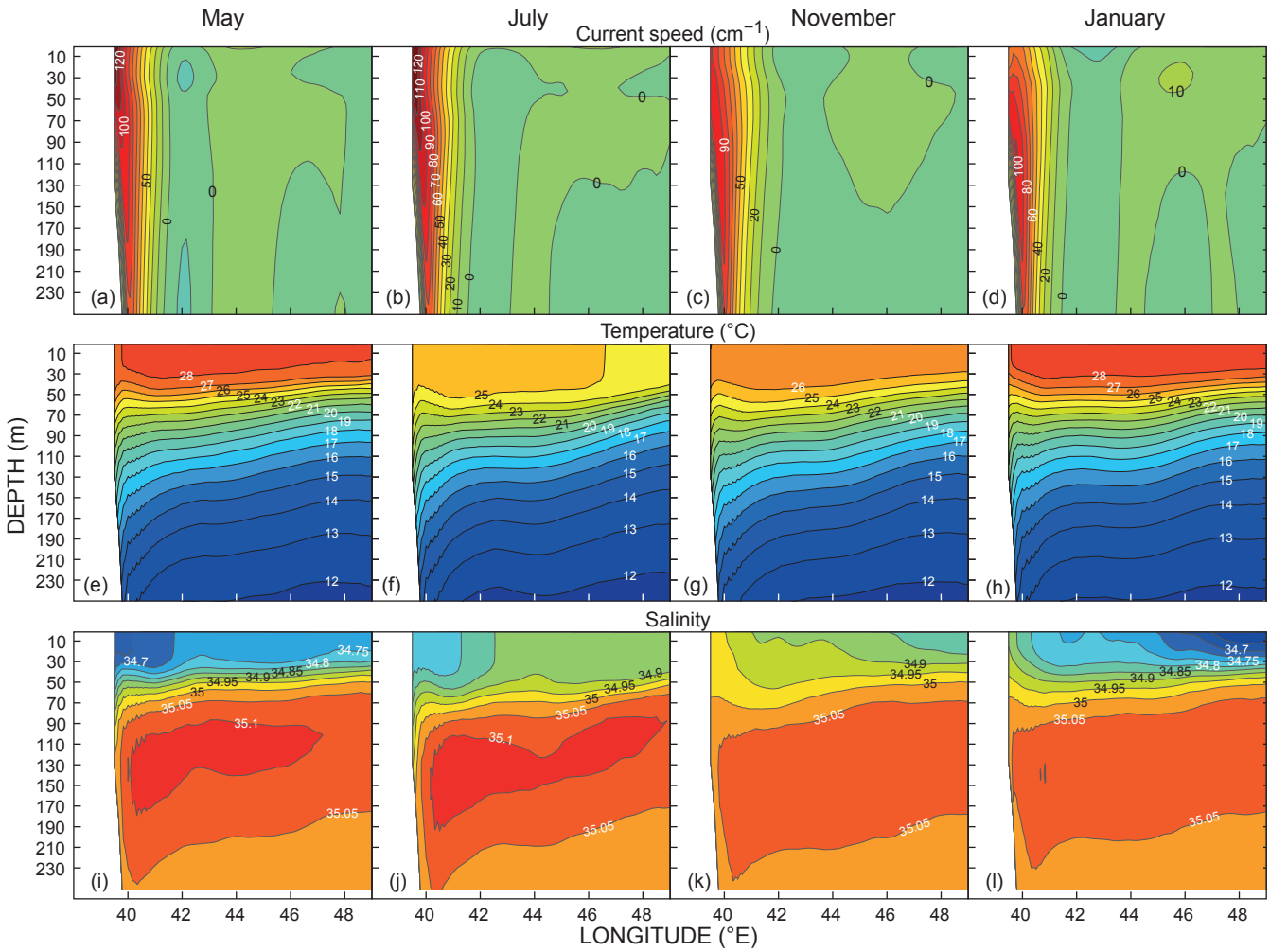

Figure 13: Vertical sections of (a–d) alongshore current component (10 cm s^{-1} contour intervals), (e–h) temperature (1 °C contour intervals) and (i–l) salinity (0.05 contour intervals) averaged over 7–7.5° S from near 40° E to 49° E for Model_NCEP

these months, the EACC is fairly weak, with the strongest values being confined to the subsurface (Figure 13c, d). In November, the surface waters have a constant temperature of about 26–26.5 °C within the upper 50 m, whereas the isohalines of about 34.8–35.0 are vertically displaced towards the surface, and also towards the coast. This period is characterised by weak winds that reduce the wind-induced evaporative heat losses and vertical mixing, resulting in warmer surface temperatures than in July. In January, the EACC is weakened, especially at the surface, with strong speeds located in the subsurface waters. The vertical temperature and salinity distributions show warm and fresh surface waters with near-horizontal isotherms and isohalines, except near the coast where they are vertically displaced upward. Warmer waters of about 28 °C appear at the surface, being vertically displaced upward over the shelf near the coast. Moreover, the warmer waters are displaced upward from about 100 m depth, being associated with weak upwelling of warm waters due to the northerly/north-easterly wind component along the Tanzanian coast. The effects of upwelling in the Tanzanian shelf waters are more apparent in the vertical structure of salinity than in temperature in January. This is shown by the salty waters (salinity about 34.9) being vertically displaced upward towards the shelf and surface near the coast from 50 m depth in November and January.

Discussion and conclusion

The tropical western Indian Ocean experiences a strong annual cycle, which influences fishing, shipping and oil and gas exploration and hence the regional economy. Strong south-westerly and north-easterly winds blow during the South-West Monsoon and North-East Monsoon from and to the tropical western Indian Ocean, respectively. During these seasons, the tropical western Indian Ocean experiences strong seasonality in the upper-ocean dynamics, which is driven by corresponding strong seasonally reversing winds. During the South-West Monsoon, the south-east trade winds along the Tanzanian and northern Mozambique coasts strengthen the EACC to its maximum speeds, which then supplies the northward-flowing SC that flows across the equator and turns offshore to the east. The EACC is weakened during the North-East Monsoon

by the north-easterly winds and the southward-flowing SC. The transition seasons occur in April–May and October–November, with weak surface winds that are dominated by a westerly component along the equator (Schott et al. 2009). Given the very limited observations in the region (e.g. Newell 1957; Dubi 2000; Julius 2005), numerical model analyses as presented here provide a better understanding of the annual cycle of the upper-ocean dynamics and their influences on the ocean properties in the tropical western Indian Ocean.

Two realistic ROMS configurations have been used to assess the mean state and annual cycle of the upper-ocean dynamics in the tropical western Indian Ocean; namely, the COADS run and NCEP run. The evaluation of the mean state and annual cycle of the upper-ocean circulation in the tropical western Indian Ocean shows good consensus between the model simulations, previous studies, satellite data and observational data. The modelled ocean currents and SSH were compared with the AVISO data. The model performance in reproducing the mean state and annual cycle in the tropical western Indian Ocean was shown to be in reasonably good agreement with satellite-derived data.

The upper-ocean dynamics in the tropical western Indian Ocean show spatial differences in the mean state. Strong, positive (anticyclonic) wind stress curl appears to the north of Madagascar and extends towards the Tanzanian coast, and is associated with generally equatorward wind stress. Thus, the anticyclonic wind stress curl results in Ekman convergence and consequently downwelling between the north of Madagascar and the Tanzanian coast. Strong currents occur along the East African coast and to the north of Madagascar; the EACC and the NEMC, respectively. The mean speeds of the model NEMC are in agreement with the observed 70 cm s^{-1} reported by Schott and McCreary (2001) and the patterns are consistent with Bell (1972) and McClanahan (1988). The mean model volume transport in the Tanzanian region depicts an eastward flow into the basin-wide cyclonic tropical gyre that comprises the SEC to the south, the EACC to the west and an eastward flow to the north. The latter occurs as the SECC in austral summer and the Wyrtki jets in transition seasons, whereas in austral winter the northern boundary of this gyre lies north of the equator. An annual volume transport of about 25–35 Sv occurs to the north of Madagascar in the model runs which reflects the NEMC, and they agree reasonably well with the value of 29.60 Sv reported by Swallow et al. (1988) and Schott et al. (2009). The annual mean volume transported by the EACC in the model appears to be 20–25 Sv.

Seasonality in the upper-ocean dynamics occurs between Tanzanian shelf waters and that to the north of Madagascar, where the NEMC and the EACC are in phase throughout the year. The volume transport of the NEMC and the EACC peaks in June through July in the model forced by NCEP reanalysis. Both model simulations indicate positive (anticyclonic) wind stress curl, indicative of downwelling throughout the year to the north-west of Madagascar and extending to Tanzanian coastal waters, as suggested by Bell (1972) and McClanahan (1988). The most negative SSH values appear around 8° S in the region between the SEC and SECC (Donguy and Meyers 1995). Throughout the year, high SSH values occur south of 10° S near the Tanzanian coast and the most negative (lowest) SSH values appear to the south between 5° and 12° S with an elongated and contracted shape. The SSH difference between high and low sea levels in the domain is >40 cm throughout the year, implying a dynamically active region year-round.

The variability of the volume transport, the ocean currents, temperature and salinity to the north of Madagascar along the path of the NEMC mirrors that of the EACC along the central Tanzanian shelf throughout the year. This suggests that the westward-flowing NEMC plays a role in determining the temperature and salinity distributions to the north of Madagascar towards the Tanzanian shelf. The NEMC seems to influence the water masses, with cooler and lower-salinity water during the South-West Monsoon, and warmer and saltier water during the North-East Monsoon. Such distribution may be attributed to advection or to interruption of the upwelled water from the SCTR (Hermes and Reason 2008; Yokoi et al. 2008). The EACC on the Tanzanian shelf transports warm surface waters northwards during May, November and January, and cool waters in July, coinciding with the timing of the temperature changes in the westward transport of the NEMC. Furthermore, the EACC respectively transports the lowest and highest surface salinity northwards in May and November, the same months of westward transport of these fresher and saltier waters by the NEMC. However, precipitation and river run-off contributions to the water budget in the region are not explicitly considered here, and should be considered in future studies.

The tropical western Indian Ocean has been shown to be a dynamically active region throughout the year in terms of the wind stress curl, Ekman transport, near-surface currents, SSH and volume transport. Such dynamical activeness influences marine industries in the region, which significantly contribute to the socio-economic development of the neighbouring countries and is therefore important to understand.

Acknowledgements — The model data for this study can be obtained by contacting the corresponding author (MM). The bathymetry data were derived from ETOPO2V2C, available at www.ngdc.noaa.gov. The altimeter products were generated by Salto/Duacs and distributed by AVISO, and they are available at www.aviso.oceanobs.com. Thanks are due to the Carnegie-IAS Regional Initiative in Science and Education through the Western Indian Ocean Regional Initiative in Marine Science and Education network for funding this research and the PhD of MM at the University of Cape Town.

References

Anderson DLT, Carrington DJ. 1993. Modelling interannual variability in the Indian Ocean using momentum fluxes from the operational weather analyses of the United Kingdom Meteorological Office and European Centre for Medium Range Weather Forecasts. *Journal of Geophysical Research* 98: 12483–12499.

Backeberg BC, Reason CJC. 2010. A connection between the South Equatorial Current north of Madagascar and Mozambique Channel Eddies. *Geophysical Research Letters* 37: L04604.

Bell BE. 1972. Marine fisheries. In: Morgan WTW (ed.), *East Africa: its people and resources*. London: Oxford University Press. pp 243–254.

Carton JA, Giese BS. 2008. A reanalysis of ocean climate using simple ocean data assimilation (SODA). *Monthly Weather Review* 136: 2999–3017.

Collins C, Hermes JC, Reason CJC. 2014. Mesoscale activity in the Comoros Basin from satellite altimetry and a high-resolution ocean circulation model. *Journal of Geophysical Research* 119: 4745–4760.

Collins C, Reason CJC, Hermes JC. 2012. Scatterometer and reanalysis wind products over the western tropical Indian Ocean. *Journal of Geophysical Research* 117: C03045.

Conkright ME, Locarnini RA, Garcia HE, O'Brien TD, Boyer TP, Stephens C, Antonov JI. 2002. World Ocean Atlas 2001: objective analyses, data statistics, and figures, CD-ROM documentation. Internal report. National Oceanographic Data Center, Silver Spring, Maryland.

Cutler AN, Swallow JC. 1984. Surface currents of the Indian Ocean (to 25°S, 100°E): compiled from historical data archived by the meteorological office, Bracknell, UK. *IOS Report* No. 187. Wormley: Institute of Oceanographic Sciences.

da Silva AM, Young CC, Levitus S. 1994. *Atlas of surface marine data 1994. Volume 1: algorithms and procedures.* NOAA Atlas NESDIS 6. Washington, DC: US Department of Commerce, NOAA, NESDIS.

Debreu L, Marchesiello P, Penven P, Cambon G. 2012. Two-way nesting in split-explicit ocean models: algorithms, implementation and validation. *Ocean Modelling* 49–50: 1–21.

de Ruijter WPM, Ridderinkhof H, Lutjeharms JRE, Schouten MW, Veth C. 2002. Observations of the flow in the Mozambique Channel. *Geophysical Research Letters* 29: 140-1–140-3.

de Ruijter WPM, van Aken HM, Beier EJ, Lutjeharms JRE, Matano RP, Schouten MW. 2004. Eddies and dipoles around south Madagascar: formation, pathways and large-scale impact. *Deep-Sea Research I* 51: 383–400.

Donguy JR, Meyers G. 1995. Observations of geostrophic transport variability in the western tropical Indian Ocean. *Deep-Sea Research I* 42: 1007–1028.

Donohue KA, Toole JM. 2003. A near-synoptic survey of the southwest Indian Ocean. *Deep-Sea Research II* 50: 1893–1931.

Dubi AM. 2000. Coastal erosion. In: Ngusaru AS (ed.), The present state of knowledge of marine science in Tanzania: synthesis report. Tanzania Coastal Management Partnership, and the Science and Technical Working Group. pp 5–42.

Ducet N, Le Traon PY, Reverdin G. 2000. Global high-resolution mapping of ocean circulation from TOPEX/Poseidon and ERS-1 and -2. *Journal of Geophysical Research* 105: 19477–19498.

Düing W, Schott F. 1978. Measurements in the source region of the Somali Current during monsoon reversal. *Journal of Physical Oceanography* 8: 278–289.

Ganachaud A, Wunsch C, Marotzke J, Toole J. 2000. The meridional overturning and large scale circulation of the Indian Ocean. *Journal of Geophysical Research* 105: 26117–26134.

Gordon GL, McClean JL. 1999. Thermohaline stratification of the Indonesian Seas: model and observations. *Journal of Physical Oceanography* 29: 198–216.

Han W, McCreary JP, Anderson DLT, Mariano AJ. 1999. On the dynamics of the eastward surface jets in the equatorial Indian Ocean. *Journal of Physical Oceanography* 29: 2191–2209.

Hermes JC, Reason CJC. 2008. Annual cycle of the South Indian Ocean (Seychelles-Chagos) thermocline ridge in a regional ocean model. *Journal of Geophysical Research* 113: C04035.

Jensen TG. 2003. Cross-equatorial pathways of salt and tracers from the northern Indian Ocean: modelling results. *Deep-Sea Research II* 50: 2111–2127.

Jiddawi NS, Öhman MC. 2002. Marine fisheries in Tanzania. *Ambio* 31: 518–527.

Johnson DR, Nguli MM, Kimani EJ. 1982. Response to annually reversing monsoon winds at the southern boundary of the Somali Current. *Deep-Sea Research* 29: 1217–1227.

Julius A. 2005. Monitoring programme for resource condition, environmental and biological parameters for Mnazi Bay Ruvuma estuary marine park (MBREMP), Tanzania. Final Project, Fisheries Training Programme. The United Nations University, Iceland.

Kabanova JG. 1968. Primary production in the northern part of the Indian Ocean. *Oceanology* 8: 214–255.

Large WG, McWilliams JC, Doney SC. 1994. Oceanic vertical mixing: a review and a model with a non-local boundary layer parameterization. *Reviews of Geophysics* 32: 363–403.

Leetmaa A, Quadfasel DR, Wilson D. 1982. Development of the flow field during the onset of the Somali Current, 1979. *Journal of Physical Oceanography* 12: 1325–1342.

Maltrud ME, Smith RD, Semtner AJ, Malone RC. 1998. Global eddy-resolving ocean simulation driven by 1985–1995 atmospheric winds. *Journal of Geophysical Research* 103: 30825–30853.

Manyilizu M, Dufois F, Penven P, Reason C. 2014. Interannual variability of sea surface temperature and circulation in the tropical western Indian Ocean. *African Journal of Marine Science* 36: 233–252.

Marchesiello P, McWilliams JC, Shchepetkin A. 2001. Open boundary condition for long-term integration of regional oceanic models. *Ocean Modelling* 3: 1–20.

Mayorga-Adame CG, Strub PT, Batchelder HP, Spitz YH. 2016. Characterizing the circulation off the Kenyan-Tanzanian coast using an ocean model. *Journal of Geophysical Research* 121: 1377–1399.

McClanahan TR. 1988. Seasonality in East Africa's coastal waters. *Marine Ecology Progress Series* 44: 191–199.

McCreary JP, Kundu PK, Molinari RL. 1993. A numerical investigation of dynamics, thermodynamics and mixed-layer processes in the Indian Ocean. *Progress in Oceanography* 31: 181–244.

McPhaden MJ, Meyers G, Ando K, Masumoto Y, Murty VSN, Ravichandran M et al. 2009. RAMA: the research moored array for African-Asian-Australian monsoon analysis and prediction. *Bulletin of the American Meteorological Society* 90: 459–480.

Morrow R, Birol F. 1998. Variability in the southeast Indian Ocean from altimetry: forcing mechanism for the Leeuwin Current. *Journal of Geophysical Research* 103: 18529–18544.

Newell BS. 1957. A preliminary survey of the hydrography of the British East African Coastal waters. *Fishery Publications Number* 9. London: Her Majesty's Stationery Office.

Penven P, Lutjeharms JRE, Florenchie P. 2006. Madagascar: a pacemaker for the Agulhas Current system? *Geophysical Research Letters* 33: L17609.

Pickard GL, Emery WJ. 1990. *Descriptive physical oceanography* (5th edn). Oxford: Pergamon Press.

Risien CM, Chelton DB. 2008. A global climatology of surface wind and wind stress fields from eight years of QuikSCAT Scatterometer data. *Journal of Physical Oceanography* 38: 2379–2413.

Schott F, McCreary JP. 2001. The monsoon circulation of the Indian Ocean. *Progress in Oceanography* 51: 1–123.

Schott F, Swallow JC, Fieux M. 1990. The Somali Current at the equator: annual cycle of currents and transports in the upper 1 000 m and connection to neighboring latitudes. *Deep-Sea Research* 37: 1825–1848.

Schott FA, Xie SP, McCreary JP. 2009. Indian Ocean circulation and climate variability. *Reviews of Geophysics* 47: RG1002.

Shchepetkin A, McWilliams J. 2003. A method for computing horizontal pressure-gradient force in an ocean model with a non-aligned vertical coordinate. *Journal of Geophysical Research* 108(C3): 3090 (34 pp).

Shchepetkin A, McWilliams J. 2005. The regional oceanic modeling system (ROMS): a split-explicit, free-surface, topography

following coordinate oceanic model. *Ocean Modelling* 9: 347–404.
Shenoi SSC, Saji PK, Almeida AM. 1999. Near-surface circulation and kinetic energy in the tropical Indian Ocean derived from Lagrangian drifters. *Journal of Marine Research* 57: 885–907.
Smith SL, Codispoti LA. 1980. Southwest monsoon of 1979: chemical and biological response of Somali coastal waters. *Science* 209: 597–600.
Smith WHF, Sandwell DT. 1997. Global seafloor topography from satellite altimetry and ship depth soundings. *Science* 277: 1956–1962.
Song Q, Gordon AL, Visbeck M. 2004. Spreading of the Indonesian Throughflow in the Indian Ocean. *Journal of Physical Oceanography* 34: 772–792.
Swallow JC, Fieux M, Schott F. 1988. The boundary currents east and north of Madagascar: 1. Geostrophic currents and transports. *Journal of Geophysical Research* 93: 4951–4962.
Swallow JC, Schott F, Fieux M. 1991. Structure and transport of the East African Coastal Current. *Journal of Geophysical Research* 96: 22245–22267.
Tomczak M, Godfrey JS. 1994. *Regional oceanography, an introduction*. Oxford: Pergamon.
Wyrtki K. 1973. An equatorial jet in the Indian Ocean. *Science* 181: 262–264.
Yokoi T, Tozuka T, Yamagata T. 2008. Seasonal variation of the Seychelles Dome. *Journal of Climate* 21: 3740–3754.

Manuscript received May 2015, revised October 2015, accepted October 2015